



Geophysical Research Letters[®]

RESEARCH LETTER

10.1029/2025GL117046

Key Points:

- Physics constraints are developed for the neural-network parameterization of mesoscale eddy fluxes
- Dimensional scaling constraints improve offline generalization to unseen grid resolutions and depths
- New parameterization improves the representation of kinetic and potential energy online in coarse idealized and global ocean models

Supporting Information:

Supporting Information may be found in the online version of this article.

Correspondence to:

P. Perezhigin,
pp2681@nyu.edu

Citation:

Perezhigin, P., Adcroft, A., & Zanna, L. (2025). Generalizable neural-network parameterization of mesoscale eddies in idealized and global ocean models. *Geophysical Research Letters*, 52, e2025GL117046. <https://doi.org/10.1029/2025GL117046>

Received 14 MAY 2025

Accepted 22 SEP 2025

Author Contributions:

Conceptualization: Pavel Perezhigin, Alistair Adcroft, Laure Zanna
Data curation: Alistair Adcroft
Formal analysis: Pavel Perezhigin
Funding acquisition: Laure Zanna
Investigation: Pavel Perezhigin
Methodology: Pavel Perezhigin, Alistair Adcroft, Laure Zanna
Project administration: Laure Zanna
Resources: Alistair Adcroft, Laure Zanna
Software: Pavel Perezhigin, Alistair Adcroft
Supervision: Alistair Adcroft, Laure Zanna
Validation: Pavel Perezhigin
Writing – original draft: Pavel Perezhigin
Writing – review & editing: Alistair Adcroft, Laure Zanna

© 2025. The Author(s).

This is an open access article under the terms of the [Creative Commons Attribution License](#), which permits use, distribution and reproduction in any medium, provided the original work is properly cited.

Generalizable Neural-Network Parameterization of Mesoscale Eddies in Idealized and Global Ocean Models

Pavel Perezhigin¹ , Alistair Adcroft² , and Laure Zanna^{1,3} 

¹Courant Institute of Mathematical Sciences, New York University, New York, NY, USA, ²Program in Atmospheric and Oceanic Sciences, Princeton University, Princeton, NJ, USA, ³Center for Data Science, New York University, New York, NY, USA

Abstract Data-driven methods have become popular to parameterize the effects of mesoscale eddies in ocean models. However, they perform poorly in generalization tasks and may require retuning if the grid resolution or ocean configuration changes. We address the generalization problem by enforcing physics constraints on a neural network parameterization of mesoscale eddy fluxes. We found that the local scaling of input and output features helps to generalize to unseen grid resolutions and depths offline in the global ocean. The scaling is based on dimensional analysis and incorporates grid spacing as a length scale. We formulate our findings as a general algorithm that can be used to enforce data-driven parameterizations with dimensional scaling. The new parameterization improves the representation of kinetic and potential energy in online simulations with idealized and global ocean models. Comparison to baseline parameterizations and impact on global ocean biases are discussed.

Plain Language Summary Ocean models can't directly simulate eddies that are smaller than the resolution of the computational grid. The effect of these eddies is represented by parameterizations. Machine learning offers a new way to build parameterizations directly from data, however, such parameterizations may fail when tested in new, unseen scenarios. Here, we leverage physics constraints to mitigate this, generalization, problem. Specifically, we found that method of dimensional analysis can be used to constrain data-driven parameterizations to enhance their accuracy in new scenarios without the need for retraining. New parameterization is tested in a realistic ocean model and brings us closer to robust, data-driven methods for ocean and climate models.

1. Introduction

Numerical ocean models rely on parameterizations to represent the effects of physical processes smaller than the model grid spacing, which are unresolved (Christensen & Zanna, 2022; Fox-Kemper et al., 2019; Hewitt et al., 2020). Recently, there has been a growing interest in applying machine learning methods to parameterize these subgrid physics in ocean models (Bolton & Zanna, 2019; Guillaumin & Zanna, 2021; Maddison, 2024; Perezhigin, Zhang, et al., 2024; Sane et al., 2023; Yan et al., 2024; Zanna & Bolton, 2020; Zhang et al., 2023). However, developing data-driven parameterizations for ocean models is still in its early stages, and their application is often limited to idealized configurations. Deploying data-driven parameterizations in the global ocean presents several challenges, one of which is addressed in this study—the problem of generalization to unseen scenarios.

Data-driven parameterizations rely heavily on sets of training data, and their successful implementation often requires tuning when applied to a new grid resolution (Zhang et al., 2023), flow regime (Ross et al., 2023), model configuration (Perezhigin, Zhang, et al., 2024), depth, or geographical region (Gultekin et al., 2024). However, in practice, it would be desirable to have a single parameterization that performs effectively across a variety of scenarios without requiring retuning. The ability of a data-driven model to work on new (testing) data, which is distinct from the training data, is measured by the *generalization error* (Bishop & Nasrabadi, 2006; Hastie et al., 2009). Data-driven methods work best when the testing data is drawn from the same distribution as the training data. However, in geophysical applications, the distribution of physical variables can vary vastly across different scenarios—a phenomenon referred to as a *distribution shift* (Beucler et al., 2024; Gultekin et al., 2024). In this case, domain knowledge and physics constraints can be leveraged to mitigate the generalization error of data-driven models (Kashinath et al., 2021).

In this work, we demonstrate how physics constraints can be leveraged to enhance the generalization of an Artificial Neural Network (ANN) parameterization of the ocean mesoscale eddy fluxes. Following Beucler et al. (2024), we rescale features of the ANN to minimize the distribution shift. To identify a suitable normalization technique for eddy fluxes, we apply dimensional analysis and Buckingham (1914)'s Pi theorem. Specifically, we introduce a local dimensional scaling constructed from the grid spacing and velocity gradients (Prakash et al., 2022). The local scaling improves offline generalization of the ANN parameterization to unseen grid resolutions and depths, as found in the global ocean data set CM2.6 (Griffies et al., 2015). Our findings are formulated as a general algorithm that can be used to incorporate the dimensional scaling in future applications. Additional physics constraints for the ANN parameterization are enforced following Guan et al. (2022) and Srinivasan et al. (2024). We present an online evaluation of the new ANN parameterization in the GFDL MOM6 ocean model (Adcroft et al., 2019) in idealized and global configurations.

2. A Method to Constrain Neural Network With Dimensional Scaling

Here we introduce the concept of physical dimensionality and demonstrate how it can be used to constrain data-driven parameterizations. We start with a trivial example, followed by a general algorithm. Finally, we draw connections to existing approaches.

2.1. Trivial Example

Consider the case where a scalar momentum flux T (units of $\text{m}^2 \text{s}^{-2}$) can be predicted using a length scale Δ (units of m) and inverse time scale X (units of s^{-1}):

$$T = f(\Delta, X). \quad (1)$$

Equation 1 must remain invariant under rescaling the units of time and length, that is for any $\alpha, \beta > 0$, the equality must hold: $f(\alpha\Delta, \beta X) = \alpha^2\beta^2f(\Delta, X)$. However, the unit invariance can be violated when f is parameterized by neural networks. One way to enforce it is by leveraging Buckingham (1914)'s Pi theorem, which states that the dimensional equation (such as Equation 1) can be rewritten in non-dimensional form. Specifically, for a set of three dimensional variables (T, Δ, X) with two independent dimensions (length and time), there is only one (three minus two) non-dimensional variable ($\pi_1 = T/(\Delta^2 X^2)$). Thus, Equation 1 transforms to $\pi_1 = \text{const}$, or equivalently:

$$T = \Delta^2 X^2 \theta, \quad (2)$$

where θ can be interpreted as a non-dimensional Smagorinsky (1963) coefficient. A data-driven parameterization in the form of Equation 2 with a trainable parameter θ , which is constant, follows the dimensional scaling as a hard constraint, in contrast to Equation 1, which does not guarantee dimensional consistency. Equation 2 promotes generalization as it explicitly accounts for the change in the magnitude of independent variables (Δ and X), constraining the learnable part of the mapping (θ) to be on the order of unity.

2.2. General Algorithm

Extending the example above, we suggest an algorithm to enforce dimensional scaling in ANN parameterizations by preprocessing input and output features:

1. Identify the input features that contribute significantly to the accurate prediction of the output features;
2. Construct non-dimensional input and output features from a *combined* set of identified input and output features;
3. Verify that a traditional known parameterization is a special case of the constructed non-dimensional mapping.

Step 1 follows standard dimensional analysis textbooks (Barenblatt, 1996; Bridgman, 1922). Specifically, a relevant set of input features can be identified by physical intuition or through ablation studies by evaluating the gain in offline performance from including additional dimensional features in the input set. Constructing non-dimensional features is a common approach in physics-constrained data-driven parameterizations (Ling et al., 2016; Schneider et al., 2024). However, the normalization of input features is often considered separately

from the normalization of output features (Beucler et al., 2024; Christopoulos et al., 2024; Kang et al., 2023; Xie et al., 2020), unlike our proposed method (step 2 above). Additionally, the emphasis in these works is often placed on identifying normalization factors that minimize the distribution shift, while we suggest starting with identifying features responsible for the prediction (step 1). Finally, traditional parameterizations are often used to propose efficient normalization factors (Connolly et al., 2025; Kang et al., 2023; Xie et al., 2020), while we instead advocate for having traditional parameterizations as a special case (step 3, Prakash et al. (2022, 2024)).

3. Physics Constraints for Ocean Mesoscale Parameterization

Our goal is to predict the subfilter momentum fluxes of mesoscale eddies using an Artificial Neural Network (ANN) parameterization, see schematic in Figure 1a. Various physical invariances were imposed to promote generalization.

3.1. Learning Subfilter Fluxes

We consider the acceleration produced by subfilter ocean mesoscale eddies (subfilter forcing, Bolton & Zanna, 2019):

$$\partial_t \bar{\mathbf{u}} = \mathbf{S} = (\bar{\mathbf{u}} \cdot \nabla) \bar{\mathbf{u}} - \overline{(\mathbf{u} \cdot \nabla) \mathbf{u}}, \quad (3)$$

where $\mathbf{u} = (u, v)$ is the horizontal ocean velocity, $\nabla = (\partial_x, \partial_y)$ is the horizontal gradient, and $\overline{(\cdot)}$ is the horizontal filter. The subfilter forcing can be approximated (Loose, Marques, et al., 2023) as a divergence of the momentum flux:

$$\mathbf{S} \approx \nabla \cdot \mathbf{T} \quad (4)$$

where

$$\mathbf{T} = \begin{pmatrix} T_{xx} & T_{xy} \\ T_{yx} & T_{yy} \end{pmatrix} = \begin{pmatrix} \bar{u} \bar{u} - \overline{u u} & \bar{u} \bar{v} - \overline{u v} \\ \bar{u} \bar{v} - \overline{u v} & \bar{v} \bar{v} - \overline{v v} \end{pmatrix}. \quad (5)$$

We predict the three components of \mathbf{T} , namely T_{xx} , T_{xy} , T_{yy} , rather than \mathbf{S} directly, similarly to Zanna and Bolton (2020) (ZB20 hereafter) to impose momentum conservation as a hard constraint. We enforce symmetry of the tensor \mathbf{T} by predicting T_{xy} and sharing its prediction with T_{yx} , which guarantees angular momentum conservation (Griffies, 2018, Section 17.3.3), up to machine precision. We also promote rotational and reflection invariances via data augmentation (Guan et al., 2022), independently rotating each training snapshot by 90° and reflecting it along the x and y axes, resulting in $8 = 2^3$ augmented snapshots per original one.

We learn the components of \mathbf{T} by minimizing the mean squared error (MSE) loss function:

$$\mathcal{L}_{\text{MSE}} = \|(\mathbf{S} - \nabla \cdot \hat{\mathbf{T}}) \cdot m\|_2^2 / \|\mathbf{S} \cdot m\|_2^2, \quad (6)$$

where m is the mask of wet points and $\hat{\mathbf{T}}$ is the neural network prediction of the subfilter flux as discussed below. See Supporting Information S1 for further details.

3.2. Input Features

Here, we identify the input features relevant for the prediction of momentum fluxes (step 1 of the algorithm presented in Section 2.2).

Following ZB20, we consider the components of the strain-rate tensor and vorticity as input features:

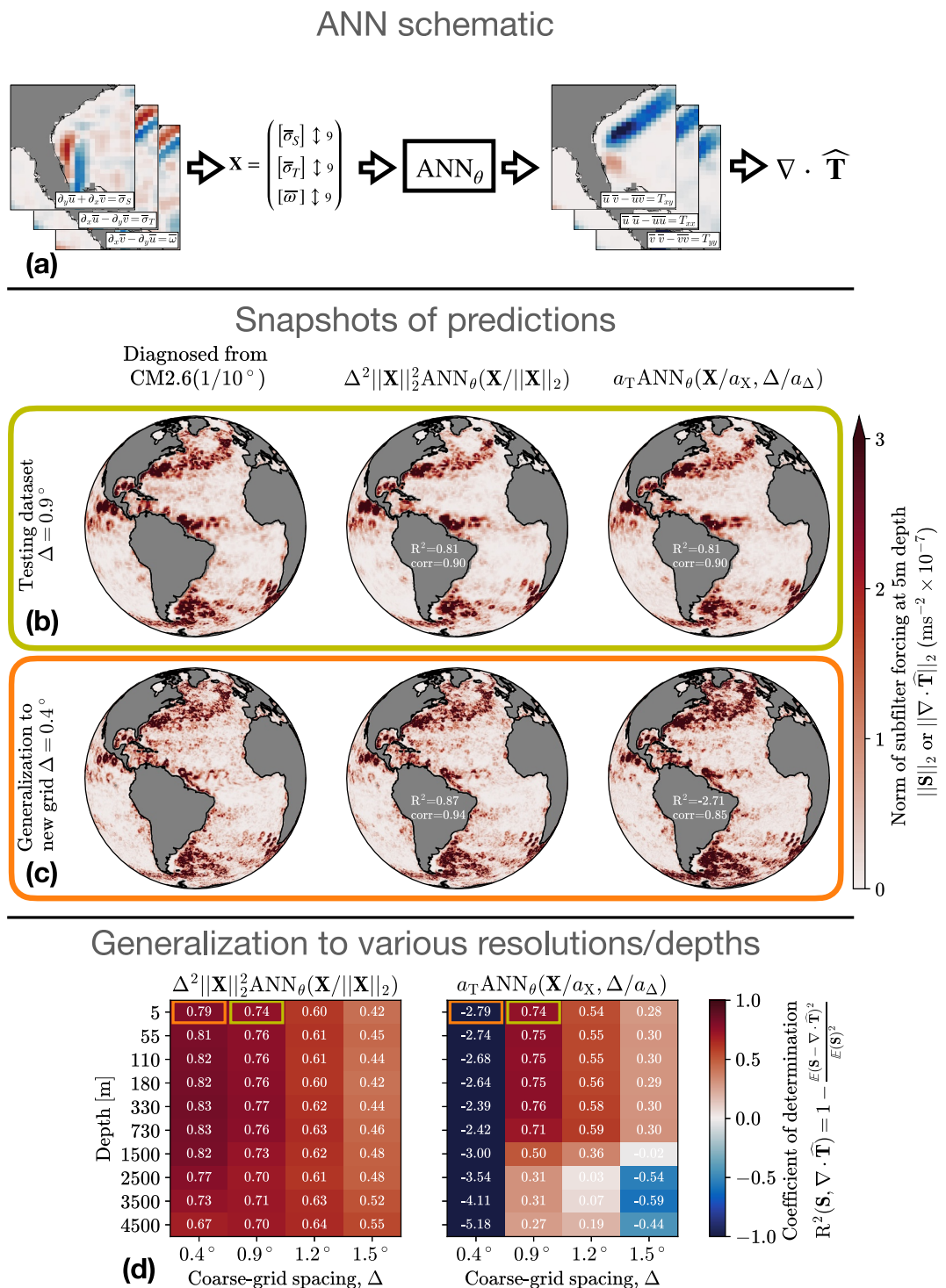


Figure 1. (a) Artificial neural network (ANN) parameterization predicting the divergence of subfilter fluxes given the velocity gradients on the horizontal stencil of 3×3 points. (b) Snapshots of predictions by two ANNs: with local dimensional scaling (Equation 11, center column) or with fixed normalization coefficients (Equation 10, right column) at the resolution (0.9°) and depth (5 m) used for training (testing data is separated by 10 years). (c) Prediction at the unseen resolution (0.4°) and the same depth (5 m). (d) Coefficient of determination (R^2) in prediction of subfilter forcing for various resolutions and depths, different from that used for training ($0.9^\circ, 5$ m). The R^2 is averaged over 2 years of held-out data and excludes 2 grid points adjacent to the coastline, where green and orange boxes correspond to panels (b, c), respectively.

$$\begin{aligned}\bar{\sigma}_S &= \partial_y \bar{u} + \partial_x \bar{v} \quad - \text{shearing strain}, \\ \bar{\sigma}_T &= \partial_x \bar{u} - \partial_y \bar{v} \quad - \text{horizontal tension/stretch}, \\ \bar{\omega} &= \partial_x \bar{v} - \partial_y \bar{u} \quad - \text{relative vorticity}.\end{aligned}\tag{7}$$

These input features exclude explicit dependence on the velocity, guaranteeing Galilean invariance of the parameterization (Ling et al., 2016; Lund & Novikov, 1993; Pope, 1975; Srinivasan et al., 2024). When using the input features (Equation 7) pointwise, the resulting ANN parameterization highly correlates with the ZB20 equation-discovery model. Thus, we decided to include the non-local contribution of these features (Gultekin et al., 2024; Maulik et al., 2019; Maulik & San, 2017; Pawar et al., 2020; Srinivasan et al., 2024; Wang et al., 2021, 2022). To do so, the input vector to the ANN consists of velocity gradients, each defined on a 3×3 horizontal stencil and flattened into a vector of length 9 (denoted as $[\cdot] \uparrow 9$):

$$\mathbf{X} = \begin{pmatrix} [\bar{\sigma}_S] \uparrow 9 \\ [\bar{\sigma}_T] \uparrow 9 \\ [\bar{\omega}] \uparrow 9 \end{pmatrix} \in \mathbb{R}^{27}.\tag{8}$$

To facilitate generalization across different resolutions (scale-aware or grid-aware parameterization, Bachman et al., 2017), we account for the local grid spacing of the coarse resolution model $\Delta = \sqrt{\Delta x \Delta y}$, resulting in the following functional form of the parameterization (Li et al., 2025; Lund & Novikov, 1993):

$$\mathbf{T} \approx \hat{\mathbf{T}}(\mathbf{X}, \Delta).\tag{9}$$

Accounting for grid spacing is physically justified as velocity gradients and momentum fluxes differ in dimensionality and require a length scale to be invoked.

3.3. Neural Network Parameterizations

We consider a baseline data-driven parameterization of eddy fluxes with fixed normalization coefficients, following the form of Equation 9:

$$\hat{\mathbf{T}}(\mathbf{X}, \Delta) = a_T \text{ANN}_\theta(\mathbf{X}/a_X, \Delta/a_\Delta),\tag{10}$$

where ANN_θ is the neural network with trainable parameters θ . Coefficients $a_T = 10^{-2} \text{ m}^2 \text{ s}^{-2}$ and $a_X = 10^{-6} \text{ s}^{-1}$ approximate the standard deviations of eddy fluxes and velocity gradients in our data set, and $a_\Delta = 50 \text{ km}$. Using fixed normalization coefficients in parameterizations similar to Equation 10 is a common practice (Srinivasan et al., 2024). Below, we contrast this approach to a normalization that follows solely from dimensional analysis presented in Section 2.2.

A combined set of input and output features $(\mathbf{T}, \mathbf{X}, \Delta)$ is used to construct non-dimensional input $(\mathbf{X}/\|\mathbf{X}\|_2)$ and output $(\mathbf{T}/(\Delta^2 \|\mathbf{X}\|_2^2))$ features (step 2 in Section 2.2), where $\|\mathbf{X}\|_2 = \sqrt{\sum_i X_i^2}$. This normalization of features is local, that is computed separately for each grid point. By designing the ANN to operate on non-dimensional variables, we propose a parameterization with the local dimensional scaling (Prakash et al., 2022; Reissmann et al., 2021):

$$\hat{\mathbf{T}}(\mathbf{X}, \Delta) = \Delta^2 \|\mathbf{X}\|_2^2 \text{ANN}_\theta(\mathbf{X}/\|\mathbf{X}\|_2).\tag{11}$$

According to the Buckingham (1914)'s Pi theorem, there is freedom in constructing non-dimensional variables. We opt to use the non-dimensional vector $\mathbf{X}/\|\mathbf{X}\|_2$ to constrain the range of its components between -1 and 1 , thereby reducing the distribution shift in ANN inputs.

Following step 3 in Section 2.2, we show that the model form (Equation 11) admits ZB20, Smagorinsky, biharmonic Smagorinsky, and Leith (1996) parameterizations as special cases, with well-behaved functional representations (see Text S1 in Supporting Information S1 for details). Furthermore, Equation 11 guarantees that the predicted fluxes vanish ($\hat{\mathbf{T}} \rightarrow \mathbf{0}$) as velocity gradients diminish ($\mathbf{X} \rightarrow \mathbf{0}$), similarly to known parameterizations, see Text S2 in Supporting Information S1. We experimentally verified that the spatial variability of the normalization factor ($\|\mathbf{X}\|_2$) in Equation 11 does not amplify the parameterization errors ($\mathbf{S} - \nabla \cdot \hat{\mathbf{T}}$) compared to Equation 10.

4. Experimental Setups

4.1. Training Data Set

The training data set is created using the climate model CM2.6 (Griffies et al., 2015), which has a nominal ocean resolution of 0.1° . Velocity gradients (Equation 7), used as input features, and subfilter forcing (\mathbf{S} , Equation 3), used as output, are diagnosed using horizontal filtering followed by coarse-graining, which avoids the inclusion of discretization errors (Agdestein & Sanderse, 2025; Christensen & Zanna, 2022; Guillaumin & Zanna, 2021). The filtering is applied by sliding a Gaussian kernel with a filter width three times the width of the target coarse grid box, using Grooms et al. (2021), Loose et al. (2022). Subsequent coarse-graining is done by averaging over the fine grid boxes contained within each coarse grid box. The filtering and coarse-graining are done for 4 coarse resolutions and 10 depth levels (Figure 1d and Table S1 in Supporting Information S1).

4.2. ANN Architecture

In the offline analysis of ANN parameterizations (Equations 10 and 11), we use a neural network with two hidden layers, 32 neurons each, which was found to be sufficiently large to effectively learn from the input features. See Text S3 in Supporting Information S1 for details.

4.3. Online Implementation

We implement the proposed ANN mesoscale eddy parameterization (Equation 11) in two considerably different configurations of the GFDL MOM6 ocean model (Adcroft et al., 2019) at eddy-permitting ($1/4^\circ$) resolution. To ensure that ANN inference remains computationally efficient, we retrain a smaller network with only one hidden layer and 20 neurons, which keeps the ANN inference time below 10% of the ocean model runtime (Text S3 in Supporting Information S1 for details). While our goal was to implement the ANN parameterization without further modifications, minor adjustments were necessary for numerical stability, see Text S4 in the Supporting Information S1.

The idealized ocean configuration, NeverWorld2 (NW2, Marques et al. (2022a, 2022b)), includes 15 stacked shallow water layers, featuring a single basin ocean with a reentrant channel. The circulation is driven by a steady wind forcing, giving rise to a circumpolar current and gyres. Coarse simulations are initialized from rest, and run for 30,000 days, similar to Marques et al. (2022a, 2022b) and Perezhogin, Zhang, et al. (2024).

The second configuration, OM4 (Adcroft et al., 2019), is a coupled ocean-sea-ice model forced at the air-sea interface by prescribing the atmosphere state according to the CORE-II interannual forcing (IAF) protocol (Large & Yeager, 2009). The simulations span 60 years (1948–2007) and were initialized with a state of the Control model after 270 years of spin-up.

The biharmonic Smagorinsky scheme for gridscale dissipation is used with viscosity coefficient $\nu_4 = 0.06\sqrt{\bar{\sigma}_S^2 + \bar{\sigma}_T^2}\Delta^4$ (Adcroft et al., 2019), applied in control and parameterized (mixed modeling, Meneveau and Katz (2000)) simulations.

5. Results

5.1. Offline Generalization

Our primary goal is to demonstrate that the local dimensional scaling promotes the generalization of the eddy parameterization to unseen grid resolutions and depths. Limited generalization in such scenarios has been

reported for previous machine-learning models of mesoscale eddies (Gultekin et al., 2024; Ross et al., 2023; Zhang et al., 2023) and traditional physics-based parameterizations (Yankovsky et al., 2024).

We compare two ANNs: one incorporating local dimensional scaling (Equation 11) and a baseline ANN with fixed normalization coefficients (Equation 10). To explore generalization, we let the ANNs learn based solely on data from one combination of depth (5 m) and coarse grid resolution (0.9°) during training. The local grid spacing varies according to the tripolar grid used in the ocean component of the CM2.6 climate model. In particular, at the nominal resolution of 0.9° , the coarse grid spacing $\Delta = \sqrt{\Delta x \Delta y}$ is in a range from 50 to 100 km for non-polar latitudes ($60S^\circ$ – $60N^\circ$). Spatially varying grid spacing provides essential information for effective learning by the baseline ANN. The offline evaluation of ANNs on held-out data similar to that used for training is shown in Figure 1b. Both ANNs exhibit high and equal pattern correlation (0.90) and R^2 (0.81) in the prediction of the norm of subfilter forcing.

We now consider generalization to a different grid resolution, which is finer (0.4°) compared to that used for training (0.9°), see Figure 1c. The range of grid spacings in this case is beyond the range seen by a baseline ANN during training, resulting in a distribution shift between the testing and training data. The baseline ANN parameterization (Equation 10) predicts the norm of subfilter forcing at a new grid resolution with a reasonably high pattern correlation (0.85). However, the magnitude of the prediction is too large, resulting in a low R^2 (-2.71). Instead, the ANN with dimensional scaling (Equation 11) offers improved generalization capability. The proposed ANN naturally accounts for the reduction of the grid spacing and reduces the magnitude of the prediction, resulting in high pattern correlation (0.94) and R^2 (0.87) metrics (Figure 1c).

The generalization to both finer and coarser grids, and different depths, is summarized in Figure 1d. At coarser grid spacings (1.2° , 1.5°) compared to that used for training (0.9°), the local dimensional scaling again helps to achieve higher R^2 by increasing the magnitude of the prediction.

In the deep layers, the subfilter forcing and velocity gradients are approximately one order of magnitude smaller than near the surface. Thus, a baseline ANN, trained on much larger values near the surface (such as here, at depth 5 m), can lead to inaccurate predictions at depth (Figure S1 in Supporting Information S1). However, the local dimensional scaling effectively rescales the input features, thereby improving generalization to deep, unseen layers, as summarized in Figure 1d.

The major reason why baseline ANN has a poor skill at unseen resolutions and depths is the lack of training data. We verified that the generalization of the baseline ANN to various resolutions and depths can be restored if these resolutions and depths are included in the training data set. Incorporating local dimensional scaling as done in this work, therefore, requires less training data and improves out-of-distribution generalization.

5.2. Online Evaluation in the MOM6 Ocean Model

We use all available depths and grid resolutions shown in Figure 1d for training to make the implemented ANN parameterization (Equation 11) less tied to any specific resolution or depth. The retrained, smaller ANN (see Section 4.3) exhibits a slightly lower offline skill (R^2) than the version described earlier, on average, by 0.1 (Figure S5 in Supporting Information S1).

5.2.1. Idealized Configuration NeverWorld2

We first consider an idealized adiabatic ocean configuration NW2, which generates various circulation patterns similar to the global ocean but allows us to isolate the effect of mesoscale eddies. Our goal is to show that the impact of the ANN parameterization on the flow is similar to that of increasing the horizontal resolution.

Mesoscale eddies extract available potential energy, $APE = \frac{\rho}{2} \sum_k g'_k (\eta_k^2 - (\eta_k^{\text{ref}})^2)$, from the mean flow, which is then converted into the eddy kinetic energy, $EKE = \frac{\rho}{2} (\overline{|\mathbf{u}^2|} - |\overline{\mathbf{u}}|^2)$ (Salmon, 1980). Here, $\overline{(\cdot)}$ is the temporal averaging, ρ is the density, g'_k is the reduced gravity of k -th isopycnal interface, η_k is the interface height and η_k^{ref} is the state of rest with flat isopycnals. At an eddy-permitting resolution ($1/4^\circ$), this energy pathway is partially unresolved (Jansen & Held, 2014; Juricke et al., 2019; Loose, Bachman, et al., 2023; Mana & Zanna, 2014). As a result, the coarse ocean model has too low EKE and too large APE when compared to the filtered and coarse-

grained high-resolution simulation, denoted as $1/32^\circ$ (Figures 2a–2c). However, Figure 2a suggests that the missing eddies can be nominally resolved on the coarse grid. Traditional backscatter parameterizations are designed to directly reduce this EKE bias by energizing the resolved eddies, resulting in additional extraction of APE (Jansen & Held, 2014; Yankovsky et al., 2024).

Eddy backscatter is diagnosed when the kinetic energy transfer produced by the subfilter forcing (Equation 3) is predominantly positive (upscale), as shown in Figure 2b. We verified that our ANN parameterization accurately predicts the eddy backscatter offline (Figure S2 in Supporting Information S1), suggesting reasonable generalization capabilities of our approach. In Figure 2e, we show a more challenging task—the prediction of the eddy backscatter online once the ANN is coupled to the coarse ocean model. The online prediction of eddy backscatter grossly resembles the diagnosed data shown in Figure 2b, although there are slight differences caused by the difference in distributions of input features.

The kinetic energy injection from the ANN parameterization leads to an increase in EKE that aligns with the high-resolution data, in particular in the ACC (Antarctic circumpolar current) region (40°S – 60°S), near the western boundaries, and in the subtropics (20°S – 20°N), see Figure 2d. However, the EKE increase in western boundary current extension (40°N , 10°E – 20°E) and subpolar gyre (50°N – 70°N) is smaller than expected from the high-resolution simulation. The spatial pattern of APE reduction in the parameterized simulation is close to that produced by increasing horizontal resolution (Figure 2f). The APE is predominantly reduced in the Southern Ocean and ACC regions (40°S – 70°S), followed by APE reduction in gyres (20°N – 60°N , 20°S – 40°S). Local patches of APE increase in the higher resolution model (Figure 2c) correspond to enhanced horizontal recirculation and are reproduced by the ANN parameterization, but less accurately compared to the diagnosed APE reduction.

Consequences of APE reduction include flattening of isopycnals and improving the structure of isopycnal interfaces across multiple cross-sections (Figure S3 in Supporting Information S1), along with a weakening of ACC transport through the Drake Passage (Table S3 in Supporting Information S1).

5.2.2. Global Ocean-Sea-Ice Model OM4

We next evaluate the ANN parameterization in the global ocean model OM4. Unlike in the idealized configuration, the interaction of many physical processes in driving the circulation in the global ocean model impede our ability to directly isolate the effect of mesoscale eddies (Ferrari & Wunsch, 2009; Lévy et al., 2010). Building on the dynamical expectations established in the idealized NW2 configuration, our goal is to assess whether the global ocean model exhibits similar response patterns to the eddy parameterization.

The prediction of the kinetic energy injection by the ANN parameterization online is shown in Figure 3a. Similarly to the idealized configuration, the kinetic energy is injected in the subtropical gyres, near the western boundaries, and occasionally in the ACC region. The energy injection is accompanied by an increase of the EKE in the same locations, see Figure 3b. However, compared to the pattern found in an idealized configuration, the EKE decrease appears more frequently: along topographic features in the subpolar gyres of the North Atlantic and North Pacific oceans, and occasionally in the ACC region. The decrease of EKE in these regions is due to a shift or weakening of the mean currents, potentially as a result of the removal of kinetic energy by the ANN parameterization along the lateral boundaries, changes in deep water formation, and/or changes in global overturning circulation. The complexity of the model prohibits us from identifying a single mechanism.

Similarly to the idealized configuration, APE is primarily reduced in the Southern Ocean (-12%), with minor APE reductions observed in the Subpolar Gyres of the North Atlantic and North Pacific oceans (Figure 3c). APE is additionally reduced in the Arctic Ocean despite the lack of increased eddy activity in this region. However, its relative change is moderately small (-2%).

We assessed whether the offline performance of the ANN parameterization correlates with the online results (Figure S5 in Supporting Information S1). We found that using spatially non-local features on a 3×3 stencil, as in this study, is important for achieving higher offline skill in CM2.6 and improved energetics in OM4 compared to a pointwise ANN parameterization and ZB20 closure. However, increasing the number of neurons, which also contributes to the offline skill, has a smaller impact on the energetics. Note that the traditional anti-viscosity

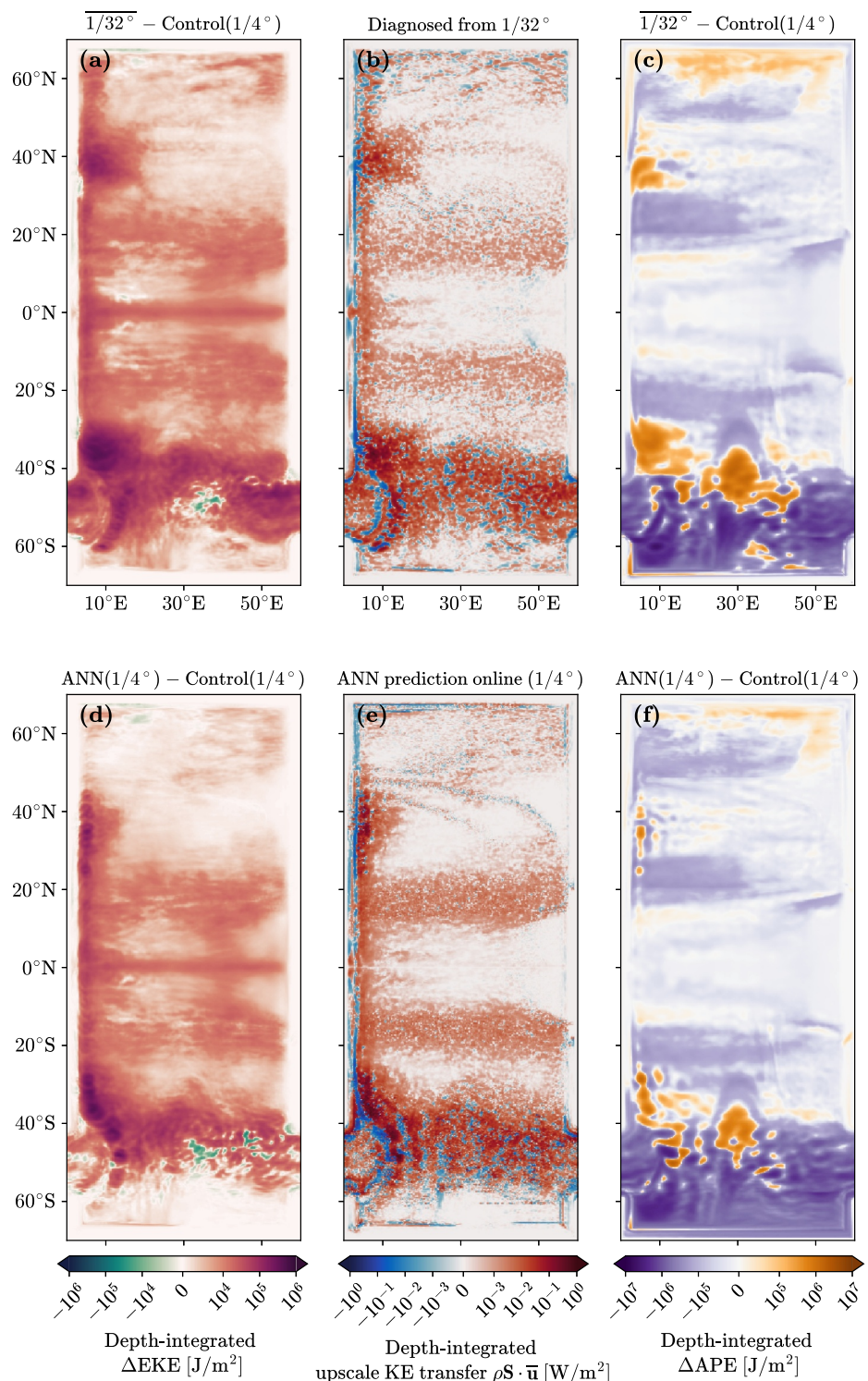


Figure 2. Simulations in idealized configuration NeverWorld2 (Marques et al., 2022a). Difference (denoted as Δ) between filtered high-resolution simulation at resolution $1/32^\circ$ and control simulation at resolution $1/4^\circ$ in (a) Eddy Kinetic Energy (EKE) and (c) Available Potential Energy (APE). (b) Upscale Kinetic Energy (KE) transfer produced by the subfilter forcing diagnosed from the high-resolution simulation (positive values represent backscatter). Difference in EKE (d) and APE (f) between the online simulation with the ANN parameterization utilizing the local dimensional scaling (Equation 11) and control simulation, both at resolution $1/4^\circ$. (e) Prediction of the KE transfer by the ANN parameterization in online simulation. All metrics are depth-integrated and averaged over 160 snapshots corresponding to the last 800 days of the simulations.

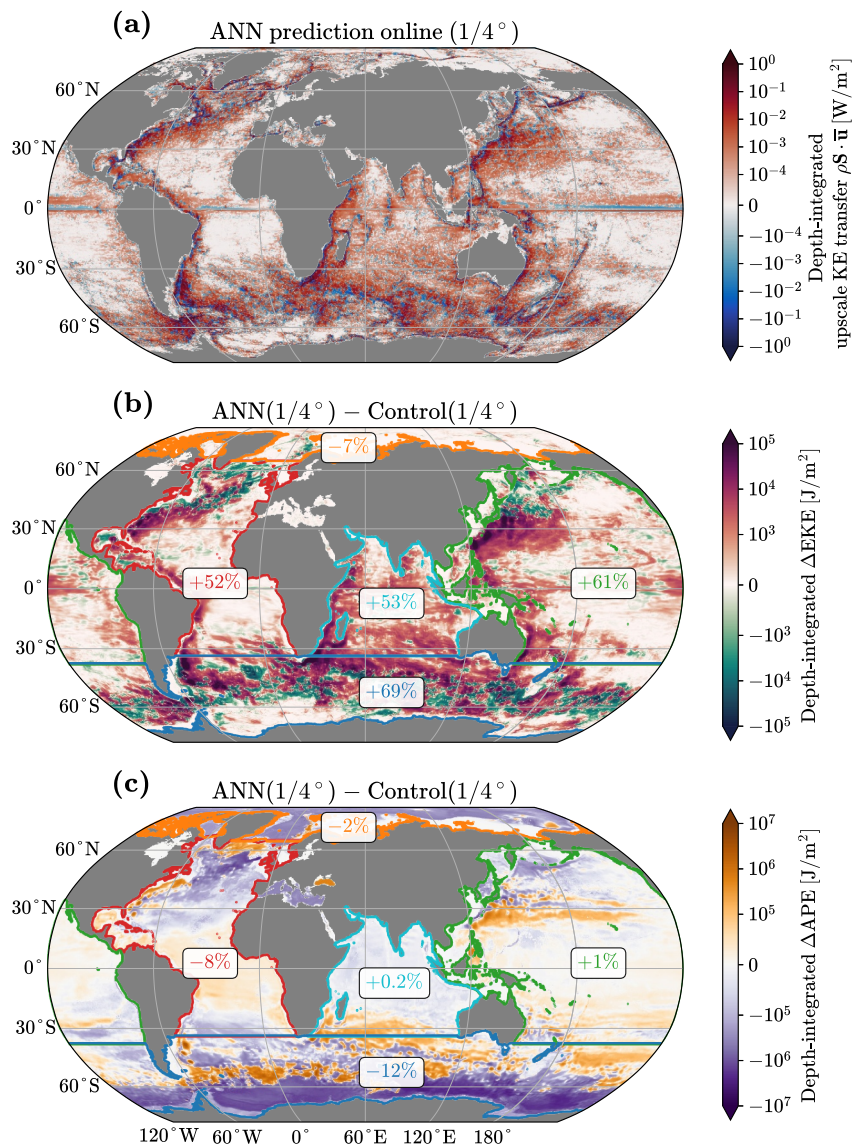


Figure 3. Online evaluation of the ANN parameterization in the global ocean-ice model OM4 (Adcroft et al., 2019) at eddy-permitting resolution ($1/4^\circ$). The following depth-integrated diagnostics are averaged over 1 year (2003): (a) upscale kinetic energy transfer predicted by the ANN parameterization online, (b) difference in Eddy kinetic energy (EKE), (c) difference in Available potential energy (APE). The integrated percentage change in EKE and APE relative to the control simulation is shown for five ocean basins.

parameterization is capable of improving energetics as well, while its offline skill is close to zero (Figure S5 in Supporting Information S1, see also Ross et al. (2023)).

We note that the evaluation presented in this section is qualitative and can be strengthened by comparing the parameterized global ocean model to filtered and coarse-grained higher-resolution simulations. Such evaluation can be performed in future studies by implementing the proposed parameterization in the hierarchy of GFDL climate models, CM4X, which differ in the horizontal resolution of the ocean component (Griffies et al., 2024).

5.2.3. Comparison to an Anti-Viscosity Parameterization

We confront our ANN parameterization to a traditional anti-viscosity parameterization representing mesoscale eddy effects (Jansen et al., 2015) and already tested in OM4 by Chang et al. (2023). Repeating their analysis, we found that both ANN and anti-viscosity parameterizations reduce the regional biases in the Gulf Stream region,

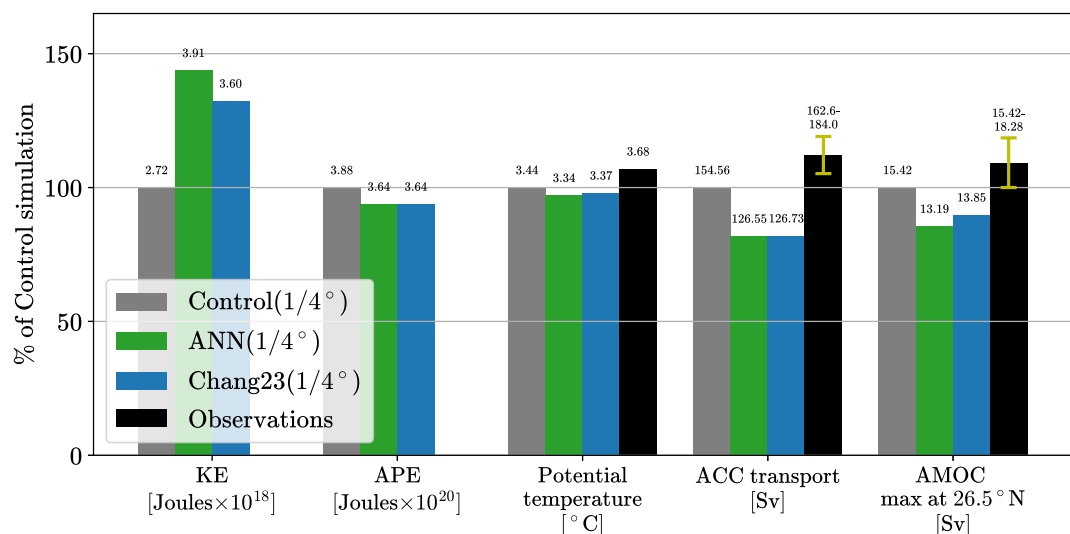


Figure 4. Comparison of the ANN parameterization to the negative viscosity backscatter parameterization (Chang et al., 2023) in the global ocean-ice model OM4. Kinetic energy (KE) and Available potential energy (APE) are integrated globally. Potential temperature is averaged globally. ACC transport is computed at the Drake Passage section at 70°W, and AMOC is computed as the maximum over depth streamfunction at 26.5°N. Model output is averaged over the years 1981–2007. Observational data for potential temperature is given by World Ocean Atlas 2018 (WOA18, Locarnini et al. (2018)), for ACC transport with error bar is given by cDrake (Donohue et al., 2016), and for AMOC is given by RAPID (Cunningham et al., 2007) averaged over 2004–2021 years with error bar showing interannual standard deviation.

see Figure S4 in Supporting Information S1 for sea surface temperature and salinity biases. The response in other global ocean circulation metrics is remarkably similar for both parameterizations as well (Figure 4). Specifically, both parameterizations increase the globally integrated kinetic energy by roughly the same percentage and reduce the APE by nearly the same percentage. The restratification effect of mesoscale eddies leads to the reduction of the globally-averaged potential temperature (Adcroft et al., 2019; Griffies et al., 2015). As previously discussed, the transport through the Drake Passage is reduced in both parameterized simulations, see also Grooms et al. (2024). Unlike in Chang et al. (2023), both parameterizations weaken the Atlantic meridional circulation (AMOC). This suggests that the AMOC response depends on the ocean model state, perhaps to a greater extent than the details of mesoscale eddy parameterizations. The response in some global metrics (ACC, AMOC, globally-averaged potential temperature) does not appear to project onto the existing ocean model biases. That is, both parameterized ocean simulations are less consistent with the observational data than the control simulation (Figure 4). We note that our goal was to improve the representation of mesoscale eddy processes. Bias reduction is not guaranteed due to compensating model errors from other parameterizations and remains an important direction for future work. A full recalibration of the ocean model may be necessary, particularly for physical processes competing with mesoscale eddies in determining average potential temperature and the strength of the ACC and AMOC.

6. Discussion

We address the generalization issue of ANN parameterizations of mesoscale eddies by embedding physics constraints into the inputs, outputs, and parametrization itself. The Buckingham (1914)'s Pi-theorem and dimensional analysis are invoked to obtain local normalization coefficients. The ANN parameterization with local dimensional scaling significantly outperforms the ANN with fixed normalization coefficients offline, demonstrating superior generalization to unseen grid resolutions and depths in the global ocean data CM2.6. A general algorithm for constructing dimensional scaling, which can be applied to other neural-network parameterizations, is presented.

The proposed ANN parameterization with dimensional scaling is successfully tested online in the GFDL MOM6 ocean model. It accurately predicts upscale kinetic energy transfer, despite many challenges presented by online implementation. The parameterization improves the energy pathways by energizing the resolved eddies and reducing APE, consistent with the expected restratification effects of mesoscale eddies. These improvements hold

across idealized (NW2) and global ocean (OM4) configurations, with the most pronounced APE reduction occurring in the Southern Ocean. The ANN achieves comparable online performance to an existing backscatter parameterization (Chang et al., 2023; Jansen et al., 2015) in OM4, and does not require significant retuning between idealized and global setups.

We demonstrate the improved or similar performance of the ANN parameterization in NW2 compared to existing backscatter schemes (Perezhogin, Zhang, et al., 2024; Yankovsky et al., 2024) across different resolutions ($1/3^{\circ}$ – $1/6^{\circ}$, see Table S2 in Supporting Information S1). At $1/2^{\circ}$, however, the ANN offers no clear improvement compared to the control simulation, likely due to less resolved eddies and stronger viscosity. At coarser resolutions ($\sim 1^{\circ}$), the subfilter momentum fluxes vanish as the Rossby radius is unresolved (Figure S6 in Supporting Information S1). At such coarse resolutions, combining the ANN with bulk parameterizations or online learning approaches may help (Maddison, 2024; Shankar et al., 2025), along with parameterizations explicitly extracting APE (Bachman, 2019; Balwada et al., 2025; Grooms et al., 2024; Jansen et al., 2019; Perezhogin, Balakrishna, & Agrawal, 2024).

Additional work is needed to enhance data-driven parameterizations beyond the performance of traditional parameterizations in realistic global configurations. Both parameterization approaches exhibit substantial departures from observations and contribute comparably to persistent model biases. This highlights the potential for improving parameterization schemes, evaluation metrics, and model calibration in ocean modeling. Looking ahead, the generalization issue addressed in this study has immediate implications for climate models, where parameterizations must remain reliable under changing conditions.

Conflict of Interest

The authors declare no conflicts of interest relevant to this study.

Data Availability Statement

The training algorithm, plots, ANN weights, implemented parameterization and MOM6 setups are available at Perezhogin (2025). The training data set, offline skill, and simulation data are available at Perezhogin et al. (2025). For high-resolution NW2 simulation data, see Marques et al. (2022b). Observational products can be found: WOA18 (Garcia et al., 2019) and RAPID (Moat et al., 2025).

Acknowledgments

This project is supported by Schmidt Sciences, LLC. LZ was also partially funded through NOAA NA19OAR4310364-T1-01. This research was also supported in part through the NYU IT High Performance Computing resources, services, and staff expertise. This research used resources of the National Energy Research Scientific Computing Center, a DOE Office of Science User Facility supported by the Office of Science of the U.S. Department of Energy under Contract No. DE-AC02-05CH11231 using NERSC award BER-ERCAP0032655. The authors would like to thank the M²LInES team, in particular, Dhruv Balwada, Alex Connolly, and Nora Loose, and also Wenda Zhang and Aviral Prakash for helpful comments and discussion. We also thank the anonymous reviewers for their helpful suggestions, which have helped improve the manuscript.

References

- Adcroft, A., Anderson, W., Balaji, V., Blanton, C., Bushuk, M., Dufour, C. O., et al. (2019). The GFDL global ocean and sea ice model OM4.0: Model description and simulation features. *Journal of Advances in Modeling Earth Systems*, 11(10), 3167–3211. <https://doi.org/10.1029/2019MS001726>
- Agdestein, S. D., & Sanderse, B. (2025). Discretize first, filter next: Learning divergence-consistent closure models for large-eddy simulation. *Journal of Computational Physics*, 522, 113577. <https://doi.org/10.1016/j.jcp.2024.113577>
- Bachman, S. D. (2019). The GM + E closure: A framework for coupling backscatter with the Gent and McWilliams parameterization. *Ocean Modelling*, 136, 85–106. <https://doi.org/10.1016/j.ocemod.2019.02.006>
- Bachman, S. D., Fox-Kemper, B., & Pearson, B. (2017). A scale-aware subgrid model for quasi-geostrophic turbulence. *Journal of Geophysical Research: Oceans*, 122(2), 1529–1554. <https://doi.org/10.1002/2016JC012265>
- Balwada, D., Perezhogin, P., Adcroft, A., & Zanna, L. (2025). *Design and implementation of a data-driven parameterization for mesoscale thickness fluxes*. AuthorPreprints.
- Barenblatt, G. I. (1996). *Scaling, self-similarity, and intermediate asymptotics: Dimensional analysis and intermediate asymptotics* (no. 14). Cambridge University Press.
- Beucler, T., Gentine, P., Yuval, J., Gupta, A., Peng, L., Lin, J., et al. (2024). Climate-invariant machine learning. *Science Advances*, 10(6), eadj7250. <https://doi.org/10.1126/sciadv.adj7250>
- Bishop, C. M., & Nasrabadi, N. M. (2006). Pattern recognition and machine learning. *Springer*, 4(4).
- Bolton, T., & Zanna, L. (2019). Applications of deep learning to ocean data inference and subgrid parameterization. *Journal of Advances in Modeling Earth Systems*, 11(1), 376–399. <https://doi.org/10.1029/2018MS001472>
- Bridgeman, P. W. (1922). *Dimensional analysis*. Yale University Press.
- Buckingham, E. (1914). On physically similar systems; illustrations of the use of dimensional equations. *Physical Review*, 4(4), 345–376. <https://doi.org/10.1103/PhysRev.4.345>
- Chang, C.-Y., Adcroft, A., Zanna, L., Hallberg, R., & Griffies, S. M. (2023). Remote versus local impacts of energy backscatter on the North Atlantic SST biases in a global ocean model. *Geophysical Research Letters*, 50(21), e2023GL105757. <https://doi.org/10.1029/2023GL105757>
- Christensen, H., & Zanna, L. (2022). *Parametrization in weather and climate models*. Oxford University Press. <https://doi.org/10.1093/acrefore/9780190228620.013.826>
- Christopoulos, C., Lopez-Gomez, I., Beucler, T., Cohen, Y., Kawczynski, C., Dunbar, O. R., & Schneider, T. (2024). Online learning of entrainment closures in a hybrid machine learning parameterization. *Journal of Advances in Modeling Earth Systems*, 16(11), e2024MS004485. <https://doi.org/10.1029/2024MS004485>

- Connolly, A., Cheng, Y., Walters, R., Wang, R., Yu, R., & Gentine, P. (2025). Deep learning turbulence closures generalize best with physics-based methods. *Authorea Preprints*. <https://doi.org/10.22541/essoar.173869578.80400701/v1>
- Cunningham, S. A., Kanzow, T., Rayner, D., Baringer, M. O., Johns, W. E., Marotzke, J., et al. (2007). Temporal variability of the Atlantic meridional overturning circulation at 26.5 N. *Science*, 317(5840), 935–938. <https://doi.org/10.1126/science.1141304>
- Donohue, K. A., Tracey, K., Watts, D. R., Chidichimo, M. P., & Chereskin, T. (2016). Mean Antarctic Circumpolar Current transport measured in Drake Passage. *Geophysical Research Letters*, 43(22), 11–760. <https://doi.org/10.1002/2016GL070319>
- Ferrari, R., & Wunsch, C. (2009). Ocean circulation kinetic energy: Reservoirs, sources, and sinks. *Annual Review of Fluid Mechanics*, 41(1), 253–282. <https://doi.org/10.1146/annurev.fluid.40.111406.102139>
- Fox-Kemper, B., Adcroft, A., Böning, C. W., Chassignet, E. P., Curchitser, E., Danabasoglu, G., et al. (2019). Challenges and prospects in ocean circulation models. *Frontiers in Marine Science*, 6, 65. <https://doi.org/10.3389/fmars.2019.00065>
- Garcia, H. E., Boyer, T. P., Baranova, O. K., Locarnini, R. A., Mishonov, A. V., Grodsky, A., et al. (2019). World Ocean Atlas 2018: Product documentation [Dataset]. <https://doi.org/10.25923/tzyw-rp36>
- Griffies, S. M. (2018). *Fundamentals of ocean climate models*. Princeton University press. <https://doi.org/10.2307/j.ctv301gzg>
- Griffies, S. M., Adcroft, A., Bealing, R. L., Bushuk, M., Chang, C.-Y., Drake, H. F., et al. (2024). The GFDL-CM4X climate model hierarchy, Part I: Model description and thermal properties. *Authorea Preprints*. <https://doi.org/10.22541/essoar.173282145.53065190/v1>
- Griffies, S. M., Winton, M., Anderson, W. G., Benson, R., Delworth, T. L., Dufour, C. O., et al. (2015). Impacts on ocean heat from transient mesoscale eddies in a hierarchy of climate models. *Journal of Climate*, 28(3), 952–977. <https://doi.org/10.1175/JCLI-D-14-00353.1>
- Grooms, I., Agarwal, N., Marques, G. M., Pégion, P., & Yassin, H. (2024). The stochastic GM+ E closure: A framework for coupling stochastic backscatter with the Gent and McWilliams parameterization. *Authorea Preprints*. <https://doi.org/10.22541/essoar.172118408.85625257/v1>
- Grooms, I., Loose, N., Abernathy, R., Steinberg, J., Bachman, S. D., Marques, G. M., et al. (2021). Diffusion-based smoothers for spatial filtering of gridded geophysical data. *Journal of Advances in Modeling Earth Systems*, 13(9), e2021MS002552. <https://doi.org/10.1029/2021MS002552>
- Guan, Y., Subel, A., Chattopadhyay, A., & Hassanzadeh, P. (2022). Learning physics-constrained subgrid-scale closures in the small-data regime for stable and accurate LES. *Physica D: Nonlinear Phenomena*, 443, 133568. <https://doi.org/10.1016/j.physd.2022.133568>
- Guillaumin, A. P., & Zanna, L. (2021). Stochastic-deep learning parameterization of ocean momentum forcing. *Journal of Advances in Modeling Earth Systems*, 13(9), e2021MS002534. <https://doi.org/10.1029/2021MS002534>
- Gultekin, C., Subel, A., Zhang, C., Leibovich, M., Perezhogin, P., Adcroft, A., et al. (2024). An analysis of deep learning parameterizations for ocean subgrid eddy forcing. *arXiv preprint arXiv:2411.06604*. <https://doi.org/10.48550/arXiv.2411.06604>
- Hastie, T., Tibshirani, R., Friedman, J. H., & Friedman, J. H. (2009). *The elements of statistical learning: Data mining, inference, and prediction* (Vol. 2). Springer.
- Hewitt, H. T., Roberts, M., Mathiot, P., Biastoch, A., Blockley, E., Chassignet, E. P., et al. (2020). Resolving and parameterising the ocean mesoscale in Earth system models. *Current Climate Change Reports*, 6(4), 137–152. <https://doi.org/10.1007/s40641-020-00164-w>
- Jansen, M. F., Adcroft, A., Khani, S., & Kong, H. (2019). Toward an energetically consistent, resolution aware parameterization of ocean mesoscale eddies. *Journal of Advances in Modeling Earth Systems*, 11(8), 2844–2860. <https://doi.org/10.1029/2019MS001750>
- Jansen, M. F., & Held, I. M. (2014). Parameterizing subgrid-scale eddy effects using energetically consistent backscatter. *Ocean Modelling*, 80, 36–48. <https://doi.org/10.1016/j.ocemod.2014.06.002>
- Jansen, M. F., Held, I. M., Adcroft, A., & Hallberg, R. (2015). Energy budget-based backscatter in an eddy permitting primitive equation model. *Ocean Modelling*, 94, 15–26. <https://doi.org/10.1016/j.ocemod.2015.07.015>
- Juricke, S., Danilov, S., Kutsenko, A., & Oliver, M. (2019). Ocean kinetic energy backscatter parametrizations on unstructured grids: Impact on mesoscale turbulence in a channel. *Ocean Modelling*, 138, 51–67. <https://doi.org/10.1016/j.ocemod.2019.03.009>
- Kang, M., Jeon, Y., & You, D. (2023). Neural-network-based mixed subgrid-scale model for turbulent flow. *Journal of Fluid Mechanics*, 962, A38. <https://doi.org/10.1017/jfm.2023.260>
- Kashinath, K., Mustafa, M., Albert, A., Wu, J., Jiang, C., Esmaeilzadeh, S., et al. (2021). Physics-informed machine learning: Case studies for weather and climate modelling. *Philosophical Transactions of the Royal Society A*, 379(2194), 20200093. <https://doi.org/10.1098/rsta.2020.0093>
- Large, W., & Yeager, S. (2009). The global climatology of an interannually varying air-sea flux data set. *Climate Dynamics*, 33(2–3), 341–364. <https://doi.org/10.1007/s00382-008-0441-3>
- Leith, C. (1996). Stochastic models of chaotic systems. *Physica D: Nonlinear Phenomena*, 98(2–4), 481–491. [https://doi.org/10.1016/0167-2789\(96\)00107-8](https://doi.org/10.1016/0167-2789(96)00107-8)
- Lévy, M., Klein, P., Trégouer, A.-M., Iovino, D., Madec, G., Masson, S., & Takahashi, K. (2010). Modifications of gyre circulation by submesoscale physics. *Ocean Modelling*, 34(1–2), 1–15. <https://doi.org/10.1016/j.ocemod.2010.04.001>
- Li, H., Xie, J., Zhang, C., Zhang, Y., & Zhao, Y. (2025). A transformer-based convolutional method to model inverse cascade in forced two-dimensional turbulence. *Journal of Computational Physics*, 520, 113475. <https://doi.org/10.1016/j.jcp.2024.113475>
- Ling, J., Kurzawski, A., & Templeton, J. (2016). Reynolds averaged turbulence modelling using deep neural networks with embedded invariance. *Journal of Fluid Mechanics*, 807, 155–166. <https://doi.org/10.1017/jfm.2016.615>
- Locarnini, M., Mishonov, A., Baranova, O., Boyer, T., Zweng, M., Garcia, H., et al. (2018). *World ocean atlas 2018, volume 1: Temperature*. NOAA Atlas NESDIS.
- Loose, N., Abernathy, R., Grooms, I., Busecke, J., Guillaumin, A., Yankovsky, E., et al. (2022). GCM-filters: A Python package for diffusion-based spatial filtering of gridded data. *Journal of Open Source Software*, 7(70), 3947. <https://doi.org/10.21105/joss.03947>
- Loose, N., Bachman, S., Grooms, I., & Jansen, M. (2023). Diagnosing scale-dependent energy cycles in a high-resolution isopycnal ocean model. *Journal of Physical Oceanography*, 53(1), 157–176. <https://doi.org/10.1175/JPO-D-22-0083.1>
- Loose, N., Marques, G. M., Adcroft, A., Bachman, S., Griffies, S. M., Grooms, I., et al. (2023). Comparing two parameterizations for the restratification effect of mesoscale eddies in an isopycnal ocean model. *Journal of Advances in Modeling Earth Systems*, 15(12), e2022MS003518. <https://doi.org/10.1029/2022MS003518>
- Lund, T. S., & Novikov, E. (1993). Parameterization of subgrid-scale stress by the velocity gradient tensor. *Annual Research Briefs*, 1992.
- Maddison, J. R. (2024). Online learning in idealized ocean gyres. *arXiv preprint arXiv:2412.06393*. <https://doi.org/10.48550/arXiv.2412.06393>
- Manz, P. P., & Zanna, L. (2014). Toward a stochastic parameterization of ocean mesoscale eddies. *Ocean Modelling*, 79, 1–20. <https://doi.org/10.1016/j.ocemod.2014.04.002>
- Marques, G. M., Loose, N., Yankovsky, E., Steinberg, J. M., Chang, C.-Y., Bhamidipati, N., et al. (2022a). NeverWorld2: An idealized model hierarchy to investigate ocean mesoscale eddies across resolutions. *Geoscientific Model Development*, 15(17), 6567–6579. <https://doi.org/10.5194/gmd-15-6567-2022>
- Marques, G. M., Loose, N., Yankovsky, E., Steinberg, J. M., Chang, C.-Y., Bhamidipati, N., et al. (2022b). Simulation data in idealized ocean configuration NeverWorld2 [Dataset]. UCAR/NCAR - CISL - CDP. <https://doi.org/10.26024/f130-ev71>

- Maulik, R., & San, O. (2017). A neural network approach for the blind deconvolution of turbulent flows. *Journal of Fluid Mechanics*, 831, 151–181. <https://doi.org/10.1017/jfm.2017.637>
- Maulik, R., San, O., Rasheed, A., & Vedula, P. (2019). Subgrid modelling for two-dimensional turbulence using neural networks. *Journal of Fluid Mechanics*, 858, 122–144. <https://doi.org/10.1017/jfm.2018.770>
- Meneveau, C., & Katz, J. (2000). Scale-invariance and turbulence models for large-eddy simulation. *Annual Review of Fluid Mechanics*, 32(1), 1–32. <https://doi.org/10.1146/annurev.fluid.32.1.1>
- Moat, B., Smeed, D., Rayner, D., Johns, W., Smith, R., Volkov, D., et al. (2025). Atlantic meridional overturning circulation observed by the RAPID-MOCHA-WBTS (RAPID-meridional overturning circulation and heatflux array-western boundary time series) array at 26N from 2004 to 2023 (v2023.1a) [Dataset]. British Oceanographic Data Centre - Natural Environment Research Council, UK. <https://doi.org/10.5285/33826d6e-801c-b0a7-e063-7086abc0b9db>
- Pawar, S., San, O., Rasheed, A., & Vedula, P. (2020). A priori analysis on deep learning of subgrid-scale parameterizations for Kraichnan turbulence. *Theoretical and Computational Fluid Dynamics*, 34(4), 429–455. <https://doi.org/10.1007/s00162-019-00512-z>
- Perezhogin, P. (2025). Generalizable neural-network parameterization of mesoscale eddies in idealized and global ocean models [Software]. Zenodo. <https://doi.org/10.5281/zenodo.16056926>
- Perezhogin, P., Adcroft, A., & Zanna, L. (2025). Generalizable neural-network parameterization of mesoscale eddies in idealized and global ocean models [Dataset]. Zenodo. <https://doi.org/10.5281/zenodo.16058005>
- Perezhogin, P., Balakrishna, A., & Agrawal, R. (2024). Large eddy simulation of ocean mesoscale eddies. In *Proceedings of the summer program 2024, center for turbulence research* (pp. 507–516). Stanford University. Retrieved from <https://arxiv.org/abs/2501.05357>
- Perezhogin, P., Zhang, C., Adcroft, A., Fernandez-Granda, C., & Zanna, L. (2024). A stable implementation of a data-driven scale-aware mesoscale parameterization. *Journal of Advances in Modeling Earth Systems*, 16(10), e2023MS004104. <https://doi.org/10.1029/2023MS004104>
- Pope, S. B. (1975). A more general effective-viscosity hypothesis. *Journal of Fluid Mechanics*, 72(2), 331–340. <https://doi.org/10.1017/S0022112075003382>
- Prakash, A., Jansen, K. E., & Evans, J. A. (2022). Invariant data-driven subgrid stress modeling in the strain-rate eigenframe for large eddy simulation. *Computer Methods in Applied Mechanics and Engineering*, 399, 115457. <https://doi.org/10.1016/j.cma.2022.115457>
- Prakash, A., Jansen, K. E., & Evans, J. A. (2024). Invariant data-driven subgrid stress modeling on anisotropic grids for large eddy simulation. *Computer Methods in Applied Mechanics and Engineering*, 422, 116807. <https://doi.org/10.1016/j.cma.2024.116807>
- Reissmann, M., Hasselberger, J., Sandberg, R. D., & Klein, M. (2021). Application of gene expression programming to a-posteriori les modeling of a Taylor green vortex. *Journal of Computational Physics*, 424, 109859. <https://doi.org/10.1016/j.jcp.2020.109859>
- Ross, A., Li, Z., Perezhogin, P., Fernandez-Granda, C., & Zanna, L. (2023). Benchmarking of machine learning ocean subgrid parameterizations in an idealized model. *Journal of Advances in Modeling Earth Systems*, 15(1), e2022MS003258. <https://doi.org/10.1029/2022MS003258>
- Salmon, R. (1980). Baroclinic instability and geostrophic turbulence. *Geophysical & Astrophysical Fluid Dynamics*, 15(1), 167–211. <https://doi.org/10.1080/03091928008241178>
- Sane, A., Reichl, B. G., Adcroft, A., & Zanna, L. (2023). Parameterizing vertical mixing coefficients in the ocean surface boundary layer using neural networks. *Journal of Advances in Modeling Earth Systems*, 15(10), e2023MS003890. <https://doi.org/10.1029/2023MS003890>
- Schneider, T., Leung, L. R., & Wills, R. C. (2024). Opinion: Optimizing climate models with process knowledge, resolution, and artificial intelligence. *Atmospheric Chemistry and Physics*, 24(12), 7041–7062. <https://doi.org/10.5194/acp-24-7041-2024>
- Shankar, V., Chakraborty, D., Viswanathan, V., & Maulik, R. (2025). Differentiable turbulence: Closure as a partial differential equation constrained optimization. *Physical Review Fluids*, 10(2), 024605. <https://doi.org/10.1103/physrevfluids.10.024605>
- Smagorinsky, J. (1963). General circulation experiments with the primitive equations: I. The basic experiment. *Monthly Weather Review*, 91(3), 99–164. [https://doi.org/10.1175/1520-0493\(1963\)091<0099:gcewtp>2.3.co;2](https://doi.org/10.1175/1520-0493(1963)091<0099:gcewtp>2.3.co;2)
- Srinivasan, K., Chekroun, M. D., & McWilliams, J. C. (2024). Turbulence closure with small, local neural networks: Forced two-dimensional and β -plane flows. *Journal of Advances in Modeling Earth Systems*, 16(4), e2023MS003795. <https://doi.org/10.1029/2023MS003795>
- Wang, Y., Yuan, Z., Wang, X., & Wang, J. (2022). Constant-coefficient spatial gradient models for the sub-grid scale closure in large-eddy simulation of turbulence. *Physics of Fluids*, 34(9), 095108. <https://doi.org/10.1063/5.0101356>
- Wang, Y., Yuan, Z., Xie, C., & Wang, J. (2021). Artificial neural network-based spatial gradient models for large-eddy simulation of turbulence. *AIP Advances*, 11(5), 055216. <https://doi.org/10.1063/5.0053590>
- Xie, C., Wang, J., & E, W. (2020). Modeling subgrid-scale forces by spatial artificial neural networks in large eddy simulation of turbulence. *Physical Review Fluids*, 5(5), 054606. <https://doi.org/10.1103/PhysRevFluids.5.054606>
- Yan, F. E., Mak, J., & Wang, Y. (2024). On the choice of training data for machine learning of geostrophic mesoscale turbulence. *Journal of Advances in Modeling Earth Systems*, 16(2), e2023MS003915. <https://doi.org/10.1029/2023MS003915>
- Yankovsky, E., Bachman, S., Smith, K. S., & Zanna, L. (2024). Vertical structure and energetic constraints for a backscatter parameterization of ocean mesoscale eddies. *Journal of Advances in Modeling Earth Systems*, 16(7), e2023MS004093. <https://doi.org/10.1029/2023MS004093>
- Zanna, L., & Bolton, T. (2020). Data-driven equation discovery of ocean mesoscale closures. *Geophysical Research Letters*, 47(17), e2020GL088376. <https://doi.org/10.1029/2020GL088376>
- Zhang, C., Perezhogin, P., Gultekin, C., Adcroft, A., Fernandez-Granda, C., & Zanna, L. (2023). Implementation and evaluation of a machine learned mesoscale eddy parameterization into a numerical ocean circulation model. *Journal of Advances in Modeling Earth Systems*, 15(10), e2023MS003697. <https://doi.org/10.1029/2023MS003697>

References From the Supporting Information

- Perezhogin, P., & Glazunov, A. (2023). Subgrid parameterizations of ocean mesoscale eddies based on Germano decomposition. *Journal of Advances in Modeling Earth Systems*, 15(10). <https://doi.org/10.1029/2023ms003771>